Catalysis Science & Technology

ROYAL SOCIETY OF CHEMISTRY

PAPER

View Article Online
View Journal | View Issue

Cite this: *Catal. Sci. Technol.*, 2024, 14, 673

A fluorolytic sol–gel route to access an amorphous Zr fluoride catalyst: a useful tool for C–F bond activation†

Christian Heinekamp, [ab] Sönke Kneiske,[b] Ana Guilherme Buzanich, [a] Mike Ahrens, [b] Thomas Braun *[b] and Franziska Emmerling *[ab]

Received 16th October 2023,
Accepted 1st January 2024

DOI: 10.1039/d3cy01439h

rsc.li/catalysis

A route to a ZrF_4 catalyst active in room temperature Friedel–Crafts and dehydrofluorination reactions was developed *via* a fluorolytic sol–gel route, which was followed by a postfluorination step using a stream of $CHClF_2$. The behaviour of different Zr(IV) precursors in a sol–gel reaction with anhydrous isopropanol/HF solution was investigated. The subsequent post-fluorination step was optimised in its temperature ramp and confirmed the necessity of a fluorination of the generated xerogels to obtain catalytic activity. The process is discussed in the context of the analysis of the materials using Brunauer–Emmett–Teller analysis (BET), powder X-ray diffraction (XRD), infrared spectroscopy (IR), thermogravimetric analysis (TGA) and differential scanning calorimetry (DSC). The local structure of the amorphous catalyst was elucidated by extended X-ray absorption fine structure spectroscopy (EXAFS).

Introduction

In the past 20 years major steps were taken in heterogeneous C–F bond activation at aluminium fluorides. The nanoscopic and amorphous aluminium chlorofluoride (ACF) was established as heterogeneous catalyst.[1–6] Subsequently, the Kemnitz group developed a fluorolytic sol–gel route to access metal fluorides[7] such as high-surface AlF_3 [8,9] and MgF_2 [10–12] which possess a high surface area. Particular in aluminium-based systems, the synthetic approach led to amorphous xerogels which can be further converted into Lewis superacids by postfluorination with Freon gas such as CCl_2F_2 (the product was then denoted as high-surface-AlF_3).[8] This progress has been crucial for the development of new materials for different catalytic applications. In general, this synthetic route offers access to metal fluorides, in addition to their respective oxides, which can be applied in heterogeneous catalysis. Before, the use of fluorides had been limited due to their small surface area, which is essential in heterogeneous catalysis to achieve high activity.[13,14] Following this breakthrough the research on aluminium based catalysts has also been extended to include other elements such as chromium,[15–17] whereas a recent approach involved the introduction of Brønsted and Lewis acidic sites into the HS-AlF_3 by using Nb doping.[19] Other approaches to AlF_3 bearing a high surface area consist of a plasma-fluorination of a zeolite precursor.[18]

Zirconium chlorofluoride (ZCF) has initially been reported to have analogous properties to ACF, but Krahl *et al.* could not confirm a comparable Lewis acidity.[20] ZCF has recently been reported as the first heterogeneous HF shuttle at room temperature.[21] Despite this knowledge, and the fact that zirconium oxide is described as a stronger Lewis acid than other metal oxides,[22] zirconium fluoride-based materials and catalysts have only recently been reported or investigated. Zirconium fluoride has been described as having Lewis-acidic properties similar to the metastable β-AlF_3 phase.[23–25] Furthermore, Lewis acidic ZrF_4 surfaces have been synthesised and characterised by George and co-workers *via* atomic layer deposition.[26] However, recent literature stated that ZrF_4 surfaces are assumed to exhibit lower Lewis acidity and lower catalytic activity compared aluminium-based based counterparts.[26,27] These results are consistent with a theoretical assessment that due to the increased size and different electronic configuration of zirconium compared to aluminium atoms a decreasing Lewis acid strength can be expected.[28]

In this work we present the development of an amorphous ZrF_4 heterogeneous catalyst which has been tested in C–F bond activation and was thoroughly characterised. The aim is

[a] *Department Materials Chemistry, Federal Institute for Material Research and Testing, Richard-Willstätter-Straße 11, 12489 Berlin, Germany. E-mail: franziska.emmerling@bam.de*
[b] *Department of Chemistry, Humboldt-Universität zu Berlin, Brook-Taylor-Straße 2, 12489 Berlin, Germany. E-mail: thomas.braun@cms.hu-berlin.de*
† Electronic supplementary information (ESI) available. See DOI: https://doi.org/10.1039/d3cy01439h

to extend the catalytic capabilities of ZrF_4. Its lower Lewis acidity is thought to be advantageous to allow better substrate desorption in catalysis.

Methods

The samples were prepared in a MBraun glovebox and all reactions were performed in JYoung NMR tubes using conventional Schlenk techniques, if not indicated otherwise. C_6D_6 was dried over K-Solvona and distilled before usage, and C_6D_{12} was purchased from Eurisotop and stored over molecular sieves. $Zr(OEt)_4$ (99%), $Zr(O^tBu)_4$ (99%) and $Zr(acac)_4$ (98+%) were obtained from Alfa Aeser, ABCR and ChemPur GmbH, respectively. ^{i}PrOH (99.5%, extra pure) was supplied by Carl-Roth, distilled and stored over molecular sieves. Triethylsilane and 1-fluoropentane were purchased from Sigma-Aldrich.

Preparation of catalysts/materials

In a typical synthesis the Zr(IV) precursor, either $Zr(OEt)_4$, $Zr(O^tBu)_4$ or $Zr(acac)_4$ (10 mmol) was placed in a flask under argon. In case of $Zr(acac)_4$ the precursor was weighed in under atmospheric conditions and placed under vacuum for 1 h in the reaction vessel before the procedure was continued. 250 mL of ^{i}PrOH were then added to the reagent. The mixture was refluxed for 1 h and allowed to cool down (Fig. 1). While the solutions including the alkoxides remained colourless the mixture obtained from $Zr(acac)_4$ appeared to be a stable milky suspension as soon as the temperature dropped below 40 °C. Subsequently, an HF solution in ^{i}PrOH (21.5 M, 4 eq.) was added dropwise, but rapidly.

The solvent was removed under vacuum, after the mixture was aged overnight under vigorous stirring. The product was stored under Ar in a glovebox. The products are designated as ZrF_3–$(F,OH)^{(OEt)}$; ZrF_3–$(F,OH)^{(O^tBu)}$ and ZrF_3–$(F,OH)^{(acac)}$, respectively. Note that due to the incomplete fluorination and residual organic content the xerogels should rather be considered as zirconium-alkoxo-fluorides ($Zr(OR)_{4-x}F_y$).

The ZrF_3–(F,OH) materials were treated further in a post-fluorination step (obtained materials are denoted as $ZrF_{4-x\ (post)}$). For this, the samples were treated under a flow of Ar and $CHClF_2$ in a temperature programmed Ni reactor (Fig. 1). For optimisation purposes the temperature program and the ratio between Ar and $CHClF_2$ were varied. A description of the parameters used can be found in Table 2.

X-ray diffraction

X-ray powder diffraction measurements were performed on an STOE Stadi MP diffractometer equipped with a Dectris Mythen 1 K linear silicon strip detector and Ge(111) double-crystal monochromator (Mo-K radiation) in a transmission geometry. The samples were prepared under Ar in a Glovebox.

High-resolution powder X-ray diffraction patterns of ZrF_3–$(F,OH)^{(acac)}$ were collected with Cu Kα radiation at a Bragg Brentano D8 Advanced diffractometer (Bruker AXS, Germany) equipped with a LYNXEYE XE-T detector. Samples were measured in reflection geometry in a 2θ range from 3° to 50° with a step size of 0.02° with spinning setup.

Crystal structure resolution calculations

The crystal structure resolution from powder diffraction data was performed *via* simulated annealing with the software EXPO2014.[29]

Infrared spectroscopy

The IR-spectra were recorded in a glovebox at a Bruker Alpha II spectrometer equipped with a diamond ATR (attenuated total reflectance) or DRIFTS (diffuse reflectance infrared Fourier transform spectroscopy) unit (Pyroelectric DTGS detector).

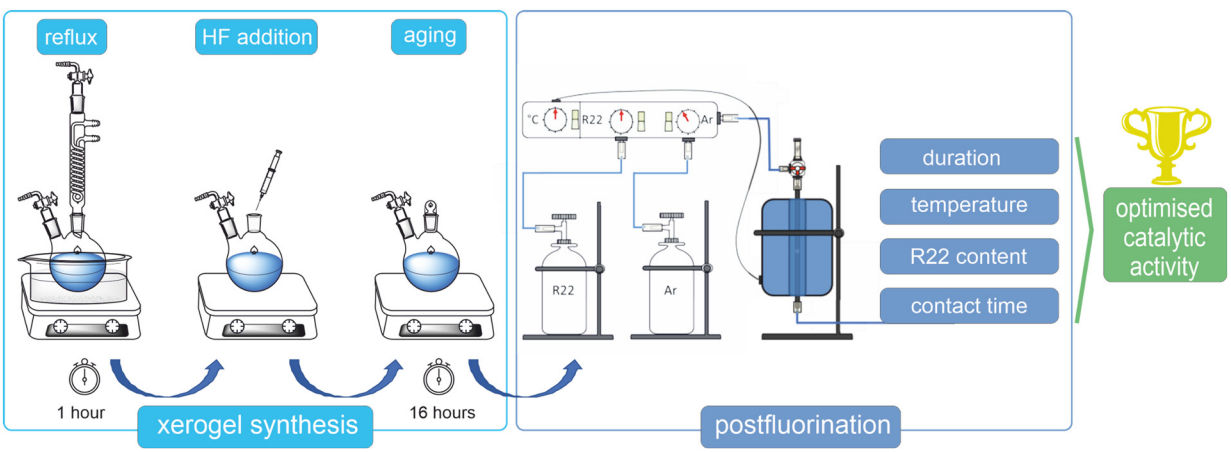

Fig. 1 Schematic representation of the xerogel synthesis and the postfluorination process presented in this work. While xerogels were synthesised in classic Schlenk apparatus (left), the postfluorination (right) was performed in a gas-flow Ni reactor, which is regulated in terms of reaction duration, temperature, fluorinating agent (R22) content and its contact time with the precatalyst.

TGA/DSC

The TGA and DSC measurements were performed at a TGA/DSC 3+ from Mettler Toledo, Switzerland. Samples were weight in in a glovebox and sealed with the A2 closing stamp. The closed crucible was pinned in a N_2 stream by the sample robot. The samples were heated from 25 to 600 °C at a rate of 10 K min^{-1}. Afterwards the samples were cooled down to 25 °C at the same rate.

N_2 gas sorption measurements

Low temperature adsorption isotherms of nitrogen at 77 K were determined with an Autosorb iQ from Anton Paar. Approximately 150 mg of the samples were tempered at 150 °C for 10 h immediately before the measurement at the device. The synthesised xerogels were tempered at 100 °C for 10 h immediately before the measurement at the device. The evaluation was carried out according to the BET theory.[30] The BJH method was used to determine the pore size. The pore volume was determined at $P/P_0 = 0.95$.[31]

EXAFS

EXAFS measurements were performed at the BAMline at BESSY-II.[32] The beam was monochromatized using a double-crystal monochromator (DCM) installed at the beamline, with a resolution ($\Delta E/E$) of about 2×10^{-4}. The slits were adjusted to provide a 4 mm (H) × 1 mm (V) spot size.

The measurements were performed at the Zr K-edge (17.889 keV) in transmission, as the sample preparation allowed choosing the adequate thickness for optimal absorption, establishing an edge jump factor of about 2. This was achieved by diluting the powder samples with boron nitride (BN). The excitation energy was varied from −200 eV to −20 eV below the edge in 10 eV steps, from −20 eV below the edge and 200 eV above the edge in 1 eV steps, and in the EXAFS region with a constant step in the k-space of 0.04 $Å^{-1}$ until k = 16 Å. EXAFS data were processed by ATHENA and ARTEMIS.[33] These GUIs programs belong to the main package IFEFFIT (v. 1.2.12). The AutoBK background subtraction procedure was used with the R_{bkg} parameter set to 1.0 Å and $k_w = 1$. Afterwards all spectra were normalized to the far post-edge region, free from absorption features. Regarding the EXFAS region, with ATHENA one can plot $\chi(k)$ against R (Å) and the oscillations represent different frequencies, which correspond to the different distances for each coordination shell. Hence, Fourier transforms (FT) are necessary for the analysis process. The FT from the k-space to R-space were performed with a Hanning-type window with a range of 1.5 Å to 14 Å. By analyzing the signal in the frequency domain in ATHENA the window range was selected to exclude the noisy part of the signal.

NMR spectroscopy

Liquid NMR spectra were measured at a Bruker DPX 300 or Bruker AVANCE II 300 spectrometer at room temperature. ^1H NMR chemical shifts δ were referenced to residual C_6D_5H (δ = 7.16 ppm) or $C_6D_{11}H$ (δ = 1.38 ppm) respectively.[19] ^{19}F NMR spectra were calibrated externally to $CFCl_3$ (δ = 0 ppm).

Reactivity studies using fluoropentane

15 mg of the respective material were placed in a JYoung NMR tube and triethylsilane (0.2 mmol) and fluoropentane (0.2 mmol) were added subsequently using a microsyringe. After that either C_6D_6 or C_6D_{12} was added to the reaction mixture. The products were analyzed by NMR spectroscopy.

Formation of $ZrF_4 \cdot CD_3CN$

The investigated sample (120 mg) was suspended in an excess of CD_3CN in a Schlenk flask and stirred at 25 °C for two hours. The excess of CD_3CN was removed under vacuum to obtain a light brown powder.

Results and discussion

A crystalline zirconium alkoxofluoride was synthesised using a strategy for xerogel synthesis previously described for aluminium fluorides. A solution of HF in ^{i}PrOH was added in stoichiometric amounts to a solution of the metal precursor in dry isopropanol. After removal of the solvent, the obtained xerogels were exposed to a postfluorination step.[34] The reaction mixtures using zirconium precursors appear as turbid gels directly after HF addition, while with aluminium alkoxides transparent gels are formed.[19] The use of different zirconium alkoxides as the metal source in the isopropanol solution does not affect the appearance of the reaction mixture. However, when the acetylacetonate complex was used a slightly different observation was made. When the mixture cooled down to room temperature it became a white suspension with a comparable viscosity compared to the hot solution. Immediately after HF addition the mixture cleared and formed an optically identical gel to the alkoxides. In all cases the xerogels were obtained as white powders. Interestingly, the xerogels obtained appear as crystalline phases (Fig. 2). Regardless of the Zr source used, the same crystalline phase is formed. This is in contrast to Al based systems which form amorphous xerogels.[8,19] The phases shown were compared with reported crystalline phases, but no match was not found in databases. In particular, the XRD pattern is dominated by a reflex at very low q, indicating a large unit cell size. The stability of the xerogel in air is longer than four months after which the powder diffraction pattern can be assigned to $ZrF_4 \cdot (H_2O)$.

The similarity between the Zr-xerogels is also revealed by the IR data (Fig. 3), as almost matching spectra were observed. Besides the broad band at 3180 cm^{-1} which can be attributed to a [ν(O–H)], typical IR bands for the isopropyl group can be detected. The IR bands between 600–800 cm^{-1} can be attributed to Zr–O vibrations, by comparing with data that have previously been calculated for Zr–O clusters.[35] Zr–F bands could not be detected as the measurement at this end

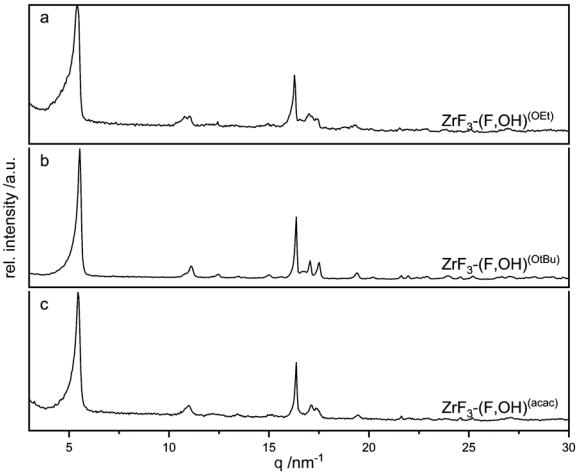

Fig. 2 Powder XRD patterns of the xerogels obtained from the respective Zr–precursor complex: (a) $Zr(OEt)_4$; (b) $Zr(O^tBu)_4$; (c) $Zr(acac)_4$.

was limited to 400 cm^{-1}.[36] The data also show bands for ^iPr residues, which suggests that a complete fluorination did not occur with HF.

Thermogravimetric analysis coupled with differential scanning calorimetry (TGA/DSC) was carried out to confirm that the organic content of all the samples was similar (Fig. 4). The TGA traces of all samples show a large weight loss of 24%, 26% and 18% respectively between 150 °C and 200 °C. While the slope of the trace for ZrF_3–$(F,OH)^{(O^tBu)}$ and ZrF_3–$(F,OH)^{(acac)}$ is distinct, the offset point for ZrF_3–$(F,OH)^{(OEt)}$ is less defined. It is likely that mainly bound isopropanol is lost. This weight loss is consistent with previous studies at Al fluoride compounds as usually a complete fluorination is not achieved by fluorolytic sol–gel synthesis.[8,19] The differences between the samples can be explained by the stability of the complex precursors. It can be assumed that some ethoxide is still bound and not fully exchanged with isopropanol leading to the initial weight loss before 150 °C mentioned above. The ^tBuO group is the one most likely to be completely exchanged by isopropanol,

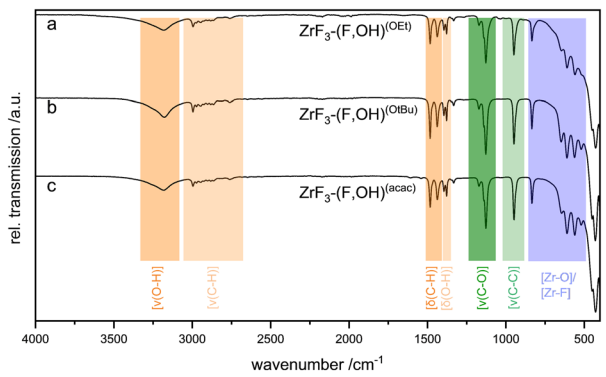

Fig. 3 ATR-FTIR spectra of the xerogels obtained from the respective Zr–precursor complex: (a) $Zr(OEt)_4$; (b) $Zr(O^tBu)_4$; (c) $Zr(acac)_4$.

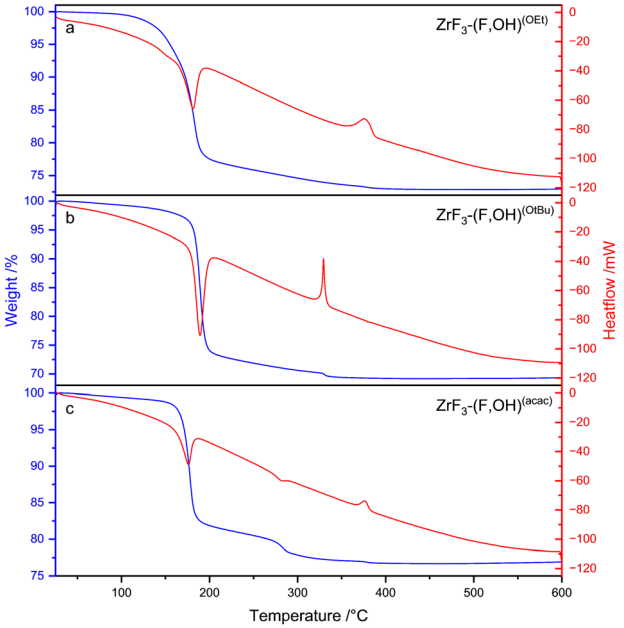

Fig. 4 TGA (blue)/DSC (red) traces from the xerogels obtained from the respective Zr–precursor complex: (a) $Zr(OEt)_4$; (b) $Zr(O^tBu)_4$; (c) $Zr(acac)_4$.

which is indicated by the larger weight loss. The xerogel derived from the $Zr(acac)_4$ complex ZrF_3–$(F,OH)^{(acac)}$ shows the lowest weight loss up to a temperature of 200 °C. As acetylacetonate is a strong chelating ligand this behaviour can be expected as it is the least likely one to be exchanged with isopropanol. Therefore, it is likely that not all of the ligands were exchanged with isopropanol.[37] Above 200 °C all samples show a steady decrease in weight up to about 400 °C, 325 °C and 380 °C respectively. The end of the weight loss is also accompanied by an exothermic process visible in the DSC trace. In addition to the steady weight loss ZrF_3–$(F,OH)^{(acac)}$ shows an additional step at approximately 280 °C, which can be attributed to the removal of residual acac ligands. Overall despite the use of different precursors to generate the samples, all samples show a similar weight loss, which is also comparable to the reported weight loss for aluminium alkoxofluorides.[8] Note that due to the incomplete fluorination and residual organic content the xerogels should rather be considered as zirconium-alkoxo-fluorides ($Zr(OR)_{4-x}F_y$) (Table 1).

As mentioned above one of the main advantages of fluorolytic sol–gel synthesis is the generation of an increased surface area of the fluorides obtained. Therefore, N_2 adsorption experiments were carried out (Fig. 5). Despite the comparable diffraction and spectroscopic data significantly different surface areas were found using BET. While ZrF_3–$(F,OH)^{(OEt)}$ shows a surface area of 300 $m^2\ g^{-1}$, ZrF_3–$(F,OH)^{(O^tBu)}$ and ZrF_3–$(F,OH)^{(acac)}$ only show surface areas of 22 $m^2\ g^{-1}$ and 26 $m^2\ g^{-1}$, respectively. ZrF_3–$(F,OH)^{(OEt)}$ does not quiet reach the values reported for the aluminium based xerogel to be 430 $m^2\ g^{-1}$, whereas the other two precursors do not even exceed the data for crystalline metal fluorides.[8]

Table 1 BET surface areas and BJH pore diameters obtained from N_2 adsorption experiments

Material	BET surface area/$m^2\ g^{-1}$	BJH pore diameter/nm
ZrF_3–$(F,OH)^{(OEt)}$	300	3
ZrF_3–$(F,OH)^{(OEt)}_{200}$	34	34
ZrF_3–$(F,OH)^{(OEt)}_{post}$	58	35
ZrF_3–$(F,OH)^{(O^tBu)}$	22	194
ZrF_3–$(F,OH)^{(O^tBu)}_{200}$	61	15
ZrF_3–$(F,OH)^{(O^tBu)}_{post}$	110	10
ZrF_3–$(F,OH)^{(acac)}$	26	34
ZrF_3–$(F,OH)^{(acac)}_{200}$	79	19
ZrF_3–$(F,OH)^{(acac)}_{post}$	63	8

In order to get a better comparison of the newly formed materials with the AlF_3 xerogels, which also loses surface area when heated without fluorinating agent, the samples were annealed under Ar atmosphere to 200 °C for 4 h. ZrF_3–$(F,OH)^{(OEt)}$ shows the expected decrease in surface area to 34 $m^2\ g^{-1}$. In contrast, ZrF_3–$(F,OH)^{(O^tBu)}$ and ZrF_3–$(F,OH)^{(acac)}$ show a significant increase in surface area to 61 $m^2\ g^{-1}$ and 79 $m^2\ g^{-1}$ after heating, respectively. This is accompanied by the presence of a type IV hysteresis for the latter samples.[38] The results indicate an organic template character which might be due to the more sterically demanding ligands, where the bound isopropoxide is removed without structural collapse.[39]

To investigate the formation of the unknown crystalline phase of the xerogels obtained from the sol–gel fluorination with HF, further xerogels were synthesized by using under-stoichiometric amounts of HF. $Zr(acac)_4$ was used as the zirconium source in the sol–gel synthesis due to the easier handling. The corresponding XRD patterns were obtained by *ex situ* XRD measurements. The obtained data show structural changes due to the different fluorination degree in the obtained materials. The addition of one equivalent led to a distinct crystalline pattern. As two equivalents of HF are used, another diffraction pattern is observed. The use of three equivalents of HF then led to the formation of a seemingly largely amorphous material, while the reflection at low q, which was also found to be prominent for the ZrF_3–$(F,OH)^{(acac)}$, was observed (see ESI† Fig. S3). This indicates that after addition of three equivalents of HF, already large periodic unit cells are formed, but the formation of larger crystallites is possibly hindered.

However, the experimental data and the current state of literature allow certain suggestions concerning the structure. Firstly, the powder XRD pattern indicates a large unit cell due to the first reflection at 6 nm^{-1}. The large unit cell can include clusters as motifs. Such oxoclusters of zirconium compounds are known to some extent.[40–42] A more recent example reports a Zr_4 motif as a Zr-oxocation.[42] Interestingly, only one example is known in literature for a Zr–F cluster, which also exhibits a four membered ring consisting of Zr coordination polyhedra with bridging F vertices (see ESI†).[43] Due to this knowledge such a cluster was postulated for a crystal structure resolution. While the modelling did not provide a structure for the acac containing xerogel, cell parameters (a = 11.422 Å, b = 5.111 Å, c = 5.803 Å, β = 91.781°, volume = 338.647 $Å^3$) for a monoclinic space group ($P2_1$) were obtained through indexing.

Xerogels obtained by the fluorolytic sol–gel process can be further fluorinated by a post-fluorination process on using freon gases.[8,44] $CHClF_2$ (R22) was used for the gas phase fluorination of ZrF_3–$(F,OH)^{(OEt)}$. To test the catalytic activity of the obtained materials after the post-fluorination, *i.e.* Friedel–Crafts reactions and dehydrofluorination reactions (Scheme 1) were performed. Both transformations have been studied previously and the activity relates to the presence of Lewis-acidic centres for activation.[45–48] In both reactions 1-fluoropentane was transformed in the presence of stoichiometric amounts of triethyl silane. In the case of the Friedel–Crafts reaction, deuterated benzene was used as a solvent acting as reagent at the same time. Regarding the dehydrofluorination reaction deuterated cyclohexane was used which is not active for Friedel–Crafts reactions.

Although both reactivities are reported in literature, it is uncommon for heterogeneous catalysts to perform at room temperature.[45–48]

Mechanistically, in both cases the silane might adsorb to the Lewis acidic centres on the surface of the catalyst forming a silylium ion species, which then activates the C–F bond of the fluoroalkane to yield a carbenium-like species. The silane then acts as hydrogen source in both the dehydrofluorination and the Friedel–Crafts reaction.[45] Hence, dihydrogen and HD are formed, respectively. Activity of both reactions could not

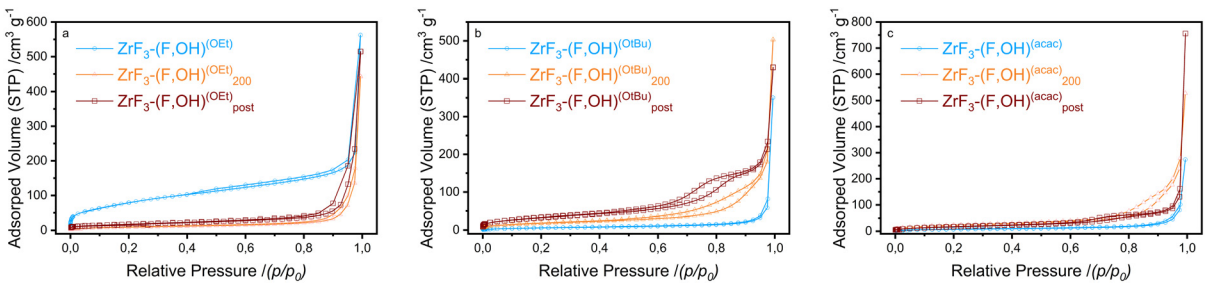

Fig. 5 N_2 adsorption and desorption isotherms at −196 °C for the synthesised xerogels, the xerogels tempered at 200 °C and the respective most active catalysts group on the respective xerogel precursor (a) ZrF_3–$(F,OH)^{(OEt)}$, (b) ZrF_3–$(F,OH)^{(O^tBu)}$, (c) ZrF_3–$(F,OH)^{(acac)}$.

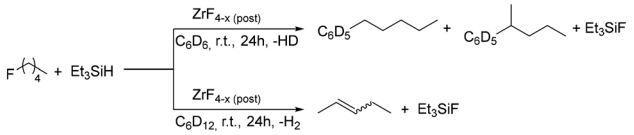

Scheme 1 Reaction scheme of Friedel–Crafts-reaction (in C_6D_6) and dehydrofluorination (in C_6D_{12}) reactivity tests at room temperature.

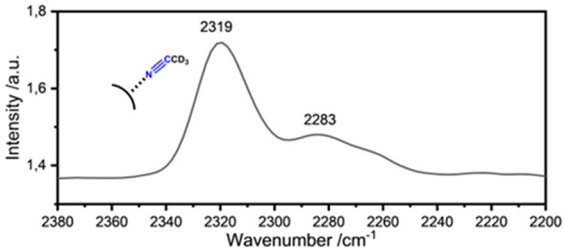

Fig. 6 DRIFTS spectrum of CD_3CN loaded ZrF_4 (entry 11).

be observed, if the xerogel was used. In the following section both reactivities are discussed in parallel.

The postfluorination which was performed in a nickel gas flow reactor (Fig. 1) using argon as carrier gas and R22 as fluorinating agent, was optimised systematically. Conditions regarding the R22 content (20%) and contact time (1.2 s) used for the postfluorination for the formation of HS-AlF_3 did not succeed for the zirconium based xerogel, leading to a slight crystalline material that does not show any catalytic activity (Table 2, entry 1). An increase of the amount of R22 in the gas stream affected the reaction mixture in two ways. Firstly, the concentration of the fluorinating agent increases. Secondly, the contact time of the gas stream with the material is reduced as the carrier gas flow is kept constant. This can lead to a contradictory situation that the reaction time is not sufficient, although more fluorinating agent is available. This effect might be the reason for lower activity of the material in catalysis when the R22 content (total fraction in the Ar/R22-gas stream) was increased to 43% (Table 2, entry 3) compared to the 33% content (Table 2, entry 2). Thus, entry 2 clearly shows significantly higher yield in both, the dehydrofluorination reaction of fluoropentane and in the Friedel–Crafts alkylation, with an additional absolute yield difference of 43%, whereas entry 3 shows equivalent but lower yields for both reactions. Interestingly, if the total postfluorination time is kept constant but the temperature is varied the "selectivity" observed for entry 2 changed to higher yields for the Friedel–Crafts alkylation (Table 2, entries 4, 6 and 7). It was observed that if the temperature regime at 240 °C is reduced or omitted, only low yields in the dehydrofluorination reaction at room temperature were found, whereas Friedel–Crafts alkylations stay above 10% (Table 2, entries 6 and 7). When the temperature program is altered to include higher temperatures or a prolonged heating at 240 °C, no activity was observed anymore.

Using the optimized conditions shown in entry 2 for ZrF_3–$(F,OH)^{(OEt)}$, the reactivity for the xerogels ZrF_3–$(F,OH)^{(O^tBu)}$ and ZrF_3–$(F,OH)^{(acac)}$ was also studied (entries 10 and 11). Overall the catalytic activity of the material that require Lewis acidic sites.[48] For the qualitative characterisation these Lewis acidic sites[49] diffuse reflectance infrared Fourier transform spectroscopy (DRIFTS) was performed at a CD_3CN adduct ZCF·CD_3CN (Table 2 entry 11; Fig. 6) The adsorption of the CD_3CN on the surface, explicitly on the acidic Lewis sites, causes a blue shift of the CN vibrational band at 2258 cm^{-1}. The extent of the observed blue shift indicates the strength of the available sites. In the DRIFTS spectrum of the post-fluorinated material described in entry 11 (Table 2) two vibrational bands can be observed after the adsorption of CD_3CN. The band at 2283 cm^{-1} ($\Delta\nu$ = 25 cm^{-1}), corresponding to very weak Lewis acidic centres. However, a band at 2319 cm^{-1} ($\Delta\nu$ = 61 cm^{-1}) can be attributed to medium to strong Lewis acidic sites.

Despite the reactivity difference for the ZrF_3–$(F,OH)^{(acac)}$ based catalyst, the yield drop observed when the ZrF_3–$(F,OH)^{(O^tBu)}$ based material was used is more significant. This change cannot be directly attributed to structural differences as

Table 2 Screening of postfluorination conditions in the gas flow reactor and the respective conversions of the obtained ZrF_{4-x} in Friedel–Crafts-alkylation and dehydrofluorination reactivity tests at room temperature

Entry	Precursor	Temperature gradient 150 °C	200 °C	240 °C	300 °C	R22 content[a]/%	Contact time/s	Yield pent-2-ene[b]/%	Yield pentylbenzene[b]/%
1[c]	ZrF_3–$(F,OH)^{(OEt)}$	1 h	2 h	2 h	—	20	1.2	0	0
2	ZrF_3–$(F,OH)^{(OEt)}$	1 h	2 h	2 h	—	33	1	82	39
3	ZrF_3–$(F,OH)^{(OEt)}$	1 h	2 h	2 h	—	43	0.85	11	11
4	ZrF_3–$(F,OH)^{(OEt)}$	1 h	3 h	1 h	—	33	1	2	9
5	ZrF_3–$(F,OH)^{(OEt)}$	1 h	1 h	3 h	—	33	1	0	0
6	ZrF_3–$(F,OH)^{(OEt)}$	1 h	4 h	—	—	33	1	0.5	18
7	ZrF_3–$(F,OH)^{(OEt)}$	5 h	—	—	—	33	1	2	11
8	ZrF_3–$(F,OH)^{(OEt)}$	1 h	2 h	3 h	—	33	1	0	0
9	ZrF_3–$(F,OH)^{(OEt)}$	1 h	2 h	—	2 h	33	1	0	0
10	ZrF_3–$(F,OH)^{(O^tBu)}$	1 h	2 h	2 h	—	33	1	25	14
11	ZrF_3–$(F,OH)^{(acac)}$	1 h	2 h	2 h	—	33	1	65	25

[a] The portion of R22 in the overall Ar/R22 gas flow. [b] Calculated by the conversion of 1-fluoropentane into the respective products by integration of the ^{1}H-NMR signals after 24 h. [c] Adapted conditions from HS-AlF_3 postfluorination.

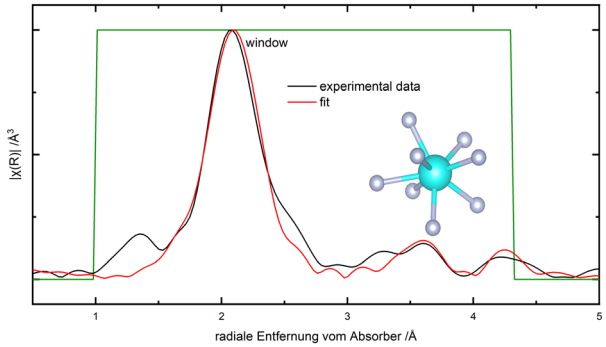

Fig. 7 EXAFS data obtained from the Zr K-edge. Magnitude of χ from Table 2 entry 2 $ZrF_{4-x\ (post)}$ using a fitting model of β-ZrF4 (*R*-factor = 0.026).

all catalysts are amorphous and knowledge about the local structure of the active site is very limited. This is supported by the IR measurements of the materials after postfluorination obtained by the conversions in the entries 10 and 11 which exhibit bands for residual organics whereas the material produced in entry 2 shows no bands in that region (see ESI†). Despite these minor IR bands visible for the $Zr(acac)_4$ and $Zr(O^t\text{-}Bu)_4$ based samples, all three materials display a very low mass loss of about 3% in TGA measurements, which indicates a very high fluorination degree. The influence of the choice of precursor on the surface area has already been mentioned. The postfluorinated xerogels ZrF_3–$(F,OH)^{(OEt)}_{post}$, ZrF_3–$(F,OH)^{(O^tBu)}_{post}$ and ZrF_3–$(F,OH)^{(acac)}_{post}$ which exhibit surface areas according to BET of 58 $m^2\ g^{-1}$, 110 $m^2\ g^{-1}$ and 63 $m^2\ g^{-1}$, respectively. All BET curves display a slight hysteresis loop according to isotherm IV (Fig. 5).[50] The reason for the significantly higher surface area of ZrF_3–$(F,OH)^{(O^tBu)}_{post}$ is unclear.

Extended X-ray absorption fine structure spectroscopy (EXAFS) was performed on the Zr-K-edge (Fig. 7) for the best performing catalyst related to the conversion shown in Table 2 entry 2. The elemental specificity of EXAFS allowed the local coordination sphere at the Zr centres to be probed. Starting from the eightfold coordination in β-ZrF_4 (ref. 24 and 51) the coordination sphere was modelled. Surprisingly, the model was able to fit up to a radial distance of more than 4 Å which begins to describe the second coordination sphere. Typically, one would expect information about the first 3 Å in such system. This means that although the material is amorphous it consists on average of similar extended local environments around the Zr centres as β-ZrF_4.

Conclusions

We have shown that active Lewis acidic zirconium fluoride catalysts are accessible *via* a fluorolytic sol–gel route. It has been revealed that the surface area of the resulting product can be influenced by the Zr source used. More importantly the use of the air-stable precursor compound $Zr(acac)_4$ was found to be a reasonable starting material for the sol–gel process, avoiding the need for air sensitive alkoxides. The synthesised catalysts obtained by postfluorination of the xerogels are active in Friedel–Crafts and dehydrofluorination reactions at room temperature. The development of defluorination processes play an important role concerning the evolving scarcity of fluorspar, the source of HF, which needs to be addressed.[52]

Author contributions

Christian Heinekamp and Sönke Kneiske performed the synthesis and analysis (NMR IR, TGA XRD). Christian Heinekamp drafted the first version of the manuscript. Ana Guilherme Buzanich performed the EXAFS measurements. The EXAFS data were jointly analysed by Christian Heinekamp and Ana Guilherme Buzanich. Structural resolution was performed by Christian Heinekamp and Franziska Emmerling. Thomas Braun, Mike Ahrens and Franziska Emmerling supervised the work and contributed to manuscript writing.

Conflicts of interest

There are no conflicts to declare.

Acknowledgements

We acknowledge financial support from the CRC 1349 "Fluorine Specific Interactions" funded by the German Research Foundation (project number 387284271). The authors thank Minh Bui for BET experiments. EXAFS experiments were performed at the BAMline at the BESSY-II storage ring (Helmholtz Center Berlin). We thank the Helmholtz-Zentrum Berlin für Materialien und Energie for the allocation of synchrotron radiation beamtime. We are thankful to Stephanos Karafiludis for helpful discussions.

Notes and references

1 T. Krahl, R. Stosser, E. Kemnitz, G. Scholz, M. Feist, G. Silly and J. Y. Buzare, *Inorg. Chem.*, 2003, **42**, 6474–6483.
2 T. Krahl and E. Kemnitz, *Angew. Chem., Int. Ed.*, 2004, **43**, 6653–6656.
3 M. C. Kervarec, T. Braun, M. Ahrens and E. Kemnitz, *Beilstein J. Org. Chem.*, 2020, **16**, 2623–2635.
4 M.-C. Kervarec, C. P. Marshall, T. Braun and E. Kemnitz, *J. Fluorine Chem.*, 2019, **221**, 61–65.
5 B. Calvo, J. Wuttke, T. Braun and E. Kemnitz, *ChemCatChem*, 2016, **8**, 1945–1950.
6 G. Meißner, K. Kretschmar, T. Braun and E. Kemnitz, *Angew. Chem.*, 2017, **129**, 16556–16559.
7 E. Kemnitz and J. Noack, *Dalton Trans.*, 2015, **44**, 19411–19431.
8 E. Kemnitz, U. Gross, S. Rudiger and C. S. Shekar, *Angew. Chem., Int. Ed.*, 2003, **42**, 4251–4254.
9 E. Kemnitz, U. Groß, S. Rüdiger and C. S. Shekar, *Angew. Chem.*, 2003, **115**, 4383–4386.
10 A. Dimitrov, S. Wuttke, S. Troyanov and E. Kemnitz, *Angew. Chem., Int. Ed.*, 2008, **47**, 190–192.

11 S. Wuttke, S. M. Coman, G. Scholz, H. Kirmse, A. Vimont, M. Daturi, S. L. M. Schroeder and E. Kemnitz, *Chem. – Eur. J.*, 2008, **14**, 11488–11499.
12 J. Krishna Murthy, U. Groß, S. Rüdiger, E. Kemnitz and J. M. Winfield, *J. Solid State Chem.*, 2006, **179**, 739–746.
13 M. Boudart, in *Handbook of heterogeneous catalysis*, Wiley-VCH, Weinheim, 2nd edn, 2008.
14 G. Busca, *Heterogeneous catalytic materials: solid state chemistry, surface chemistry and catalytic behaviour*, Elsevier, Amsterdam Heidelberg, 1st edn, 2014.
15 G. Tavčar and T. Skapin, *J. Fluorine Chem.*, 2019, **222–223**, 81–89.
16 I. K. Murwani, K. Scheurell and E. Kemnitz, *Catal. Commun.*, 2008, **10**, 227–231.
17 W. Mao, Y. Bai, Z. Jia, Y. Qin, B. Wang, W. Zhang, J. Lu and E. Kemnitz, *Dalton Trans.*, 2022, **51**, 935–945.
18 J. L. Delattre, P. J. Chupas, C. P. Grey and A. M. Stacy, *J. Am. Chem. Soc.*, 2001, **123**, 5364–5365.
19 C. P. Marshall, G. Scholz, T. Braun and E. Kemnitz, *Dalton Trans.*, 2019, **48**, 6834–6845.
20 T. Krahl and E. Kemnitz, *J. Fluorine Chem.*, 2006, **127**, 663–678.
21 C. Heinekamp, A. G. Buzanich, M. Ahrens, T. Braun and F. Emmerling, *Chem. Commun.*, 2023, **59**, 11224–11227.
22 C. Nicollet, C. Toparli, G. F. Harrington, T. Defferriere, B. Yildiz and H. L. Tuller, *Nat. Catal.*, 2020, **3**, 913–920.
23 C. L. Bailey, A. Wander, S. Mukhopadhyay, B. G. Searle and N. M. Harrison, *Phys. Chem. Chem. Phys.*, 2008, **10**, 2918–2924.
24 S. L. Benjamin, W. Levason, D. Pugh, G. Reid and W. Zhang, *Dalton Trans.*, 2012, **41**, 12548–12557.
25 A. N. Romanov, E. V. Haula, Z. T. Fattakhova, A. A. Veber, V. B. Tsvetkov, D. M. Zhigunov, V. N. Korchak and V. B. Sulimov, *Opt. Mater.*, 2011, **34**, 155–158.
26 Y. Lee, H. X. Sun, M. J. Young and S. M. George, *Chem. Mater.*, 2016, **28**, 2022–2032.
27 X. Wu, Y. Zeng, Z.-T. Jiang, Y. Zhu, L. Xie and Y. Xia, *Org. Lett.*, 2022, **24**, 8429–8434.
28 D. P. N. Satchell and R. S. Satchell, *Q. Rev., Chem. Soc.*, 1971, **25**, 171–199.
29 A. Altomare, C. Cuocci, C. Giacovazzo, A. Moliterni, R. Rizzi, N. Corriero and A. Falcicchio, *J. Appl. Crystallogr.*, 2013, **46**, 1231–1235.
30 S. Brunauer, P. H. Emmett and E. Teller, *J. Am. Chem. Soc.*, 1938, **60**, 309–319.
31 E. P. Barrett, L. G. Joyner and P. P. Halenda, *J. Am. Chem. Soc.*, 1951, **73**, 373–380.
32 A. Guilherme Buzanich, M. Radtke, K. V. Yusenko, T. M. Stawski, A. Kulow, C. T. Cakir, B. Röder, C. Naese, R. Britzke, M. Sintschuk and F. Emmerling, *J. Chem. Phys.*, 2023, **158**, 244202.
33 B. Ravel and M. Newville, *J. Synchrotron Radiat.*, 2005, **12**, 537–541.
34 C. P. Marshall, T. Braun and E. Kemnitz, *Catal. Sci. Technol.*, 2018, **8**, 3151–3159.
35 R. Jin, Y. Zhang, S. Huang, P. Wang and P. Tian, *Chin. J. Chem.*, 2011, **29**, 13–20.
36 V. Ya. Kavun, A. B. Slobodyuk, E. I. Voit, S. L. Sinebryukhov, E. B. Merkulov and V. K. Goncharuk, *J. Struct. Chem.*, 2010, **51**, 862–868.
37 D. Gibson, *Coord. Chem. Rev.*, 1969, **4**, 225–240.
38 *Characterization of porous solids and powders: surface area, pore size, and density*, Springer, Dordrecht, Boston, 2006.
39 K. J. C. van Bommel, A. Friggeri and S. Shinkai, *Angew. Chem., Int. Ed.*, 2003, **42**, 980–999.
40 F. R. Kogler, M. Jupa, M. Puchberger and U. Schubert, *J. Mater. Chem.*, 2004, **14**, 3133–3138.
41 J. Napal, B. Artetxe, G. Beobide, O. Castillo, A. Luque, J. Pascual-Colino, S. Pérez-Yáñez and M. Perfecto-Irigaray, *Inorg. Chem. Front.*, 2022, **9**, 935–940.
42 J. A. Sommers, D. C. Hutchison, N. P. Martin, K. Kozma, D. A. Keszler and M. Nyman, *J. Am. Chem. Soc.*, 2019, **141**, 16894–16902.
43 C. R. Ross, B. L. Paulsen, R. M. Nielson and S. C. Abrahams, *Acta Crystallogr., Sect. B: Struct. Sci.*, 1998, **54**, 417–423.
44 E. Kemnitz, A. Hess, G. Rother and S. Troyanov, *J. Catal.*, 1996, **159**, 332–339.
45 M. Ahrens, G. Scholz, T. Braun and E. Kemnitz, *Angew. Chem., Int. Ed.*, 2013, **52**, 5328–5332.
46 G. Meißner, D. Dirican, C. Jäger, T. Braun and E. Kemnitz, *Catal. Sci. Technol.*, 2017, **7**, 3348–3354.
47 C. P. Marshall, G. Scholz, T. Braun and E. Kemnitz, *Catal. Sci. Technol.*, 2020, **10**, 391–402.
48 M. Bui, K. Hoffmann, T. Braun, S. Riedel, C. Heinekamp, K. Scheurell, G. Scholz, T. Stawski and F. Emmerling, *ChemCatChem*, 2023, e202300350.
49 P. O. Scokart and P. G. Rouxhet, *J. Colloid Interface Sci.*, 1982, **86**, 96–104.
50 M. Thommes, K. Kaneko, A. V. Neimark, J. P. Olivier, F. Rodriguez-Reinoso, J. Rouquerol and K. S. W. Sing, *Pure Appl. Chem.*, 2015, **87**, 1051–1069.
51 C. Legein, F. Fayon, C. Martineau, M. Body, J.-Y. Buzaré, D. Massiot, E. Durand, A. Tressaud, A. Demourgues, O. Péron and B. Boulard, *Inorg. Chem.*, 2006, **45**, 10636–10641.
52 S. Bobba, S. Carrara, J. Huisman, F. Mathieux and C. Pavel, *Critical raw materials for strategic technologies and sectors in the EU—a foresight study*, 2020.

